Quantum simulation of the Kibble-Zurek mechanism using a semiconductor electron charge qubit

Li Wang,[1,*] Cheng Zhou,[1,*] Tao Tu,[1,†] Hong-Wen Jiang,[2] Guo-Ping Guo,[1,‡] and Guang-Can Guo[1]

[1]*Key Laboratory of Quantum Information, University of Science and Technology of China, Chinese Academy of Sciences, Hefei 230026, People's Republic of China*

[2]*Department of Physics and Astronomy, University of California at Los Angeles, Los Angeles, California 90095, USA*

(Received 31 July 2013; revised manuscript received 15 October 2013; published 25 February 2014)

The Kibble-Zurek mechanism is central to the nonequilibrium dynamics and topological structure that occur during phase transitions, which may be manifested as the cosmological strings of the early universe or vortex lines in a superfluid. In recent years, there has been broad interest in performing quantum simulations using different well-controlled physical setups, whose full controllability allows access to regimes that may be difficult to explore. Here, we demonstrate a proof-of-principle quantum simulation of the Kibble-Zurek mechanism in the quantum Ising model as it undergoes a quenched phase transition. We used an electron charge qubit in a double quantum dot as the simulator. We engineered the qubit under Landau-Zener dynamics and successfully reproduced the Kibble-Zurek-like dependence of the topological defect density on the quench time. The high level of tunability of two-level semiconductor systems and the intriguing analogy between the two phenomena (the Kibble-Zurek mechanism and Landau-Zener transition) offer a platform on which to gain new insight into the dynamics of various phase transitions.

DOI: 10.1103/PhysRevA.89.022337 PACS number(s): 03.67.Ac, 03.67.Lx, 05.30.Rt

I. INTRODUCTION

The Kibble-Zurek mechanism [1,2] provides a description of the nonequilibrium dynamics and the generation of topological structures, such as strings, vortices, or domain walls during symmetry-breaking phase transitions [3–9]. It should be noted that the study of the time evolution of systems undergoing phase transitions is notoriously difficult because such transitions occur very rapidly or remain intractable to calculate in many cases [10,11]. However, this difficulty may be efficiently overcome by using some controllable quantum system to study another less accessible system, i.e., quantum simulation [12–15]. The quantum simulation of the dynamics of phase transitions has been the subject of intensive discussion over the past few years [16–20]. To date, the focus has mainly been theoretical, although proof-of-concept results on the experimental side are highly desirable.

Recently, the Landau-Zener transition has been reported to exhibit the key physics of the Kibble-Zurek mechanism [21,22]. The Landau-Zener transition [23,24], occurring when a two-level system sweeps through its anticrossing point [25–28], plays a prominent role in quantum phenomena. This analogy between the two physical situations is particularly intriguing and constitutes the theoretical foundation for the implementation of quantum simulations. However, a practical scheme to construct a realizable mapping between the system and the simulator is still missing. More importantly, the experimental realization of the quantum simulation approach to mimic the quench dynamics in actual objects remains a challenge that requires a simulator designed in a fully controllable manner and with a manipulation rate much faster than the rate of decoherence. Here, we demonstrate an analog quantum simulation protocol for the Kibble-Zurek mechanism using the Landau-Zener dynamics of an electron charge qubit in a double quantum dot.

II. ANALOGY BETWEEN KIBBLE-ZUREK AND LANDAU-ZENER PROCESS

The Kibble-Zurek mechanism provides a description of the formation of topological defects during the symmetry-breaking phase transitions considered in various areas of physics, from cosmology to condensed matter [1–7] . Consider a system, shown in Fig. 1(a), traversing a second-order phase transition over a certain quench period. Here, we denote the distance from the critical point as λ. The quench process can be approximated by a time-dependent $\lambda = t/\tau_Q$, which changes linearly with time at the quenching rate $1/\tau_Q$. When the system approaches the critical point from the high-symmetry phase, the relaxation time $\tau = \tau_0/\lambda$ will diverge, which implies that the dynamics of the system becomes increasingly slow. In particular, when the relaxation time is longer than the quench time, also called the freeze-out time scale $\hat{t}_{\mathrm{KZ}}$ [2], the new broken-symmetry states are in effect immobilized, and topological defects form. Thus the density of defects ρ_{KZ}, that is the average size of the topological defects, is given by the correlation length at the freeze-out time, which is the key prediction offered by the Kibble-Zurek mechanism [2]. According to the scale of the relaxation time and quench time, the nonequilibrium phase-transition process can be distinguished into two regions in the neighborhood of the critical point: adiabatic evolution and nonadiabatic freezing.

A transition between two energy levels at the anticrossing point is known as a Landau-Zener transition [23,24]. To be more specific, in schematic Fig. 1(b), we consider a two-level system with a sweeping rate v. We denote the level of detuning as ϵ and the ground and excited states as $|0\rangle$ and $|1\rangle$, respectively. When the system approaches the anticrossing point, there is a characteristic boundary $\hat{t}_{\mathrm{LZ}}$ [25], where the energy gap E_Δ between the up and down levels is minimized relative to the sweeping rate to allow for a sudden transition

*These two authors contributed equally to this work.
†tutao@ustc.edu.cn
‡gpguo@ustc.edu.cn

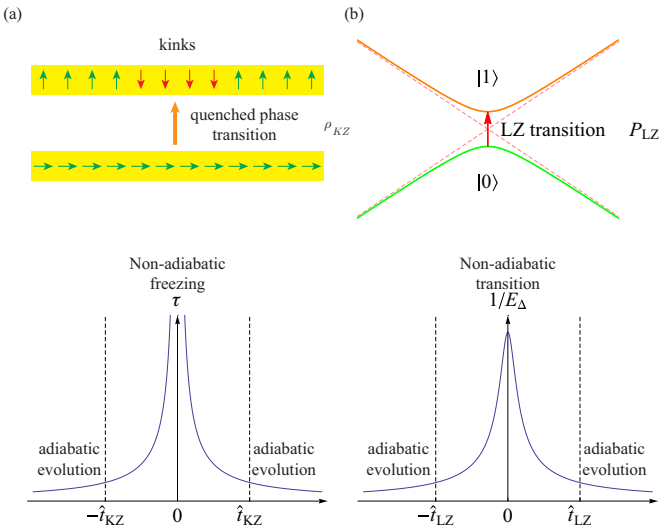

FIG. 1. (Color online) Analogy between Kibble-Zurek mechanism and Landau-Zener transition. (a) Top: schematic diagram of quenched phase transition resulting in the formation of topological defects ρ_{KZ} in a quantum Ising chain. Bottom: we can define two regions—within (outside) the time interval $[-\hat{t}_{KZ},\hat{t}_{KZ}]$, where the relaxation time τ is longer (smaller) than the quench time τ_Q such that the phase configuration will be fixed (mobile). (b) Top: illustration of the two-level system dynamics for the time-dependent sweeping. Bottom: we can also distinguish two regions—near (far from) the anticrossing point, where the inverse of the energy gap E_Δ is smaller (larger) than the sweeping rate v such that there is a nonadiabatic transition P_{LZ} between the two states (adiabatic evolution).

between the two levels. Thus it is also intuitive to use a two-stage picture [25] in which the system will evolve almost adiabatically along the ground state far from the anticrossing point and have a significant probability P_{LZ} of making a nonadiabatic transition to the excited state in the vicinity of the anticrossing point.

Compared with the two phenomena illustrated in Figs. 1(a) and 1(b), it is clear that the system undergoes a quenched phase transition from a defect-free phase to a defect phase, similar to a Landau-Zener transition from a ground state to an excited state. Here, we would like to simulate a given process (Kibble-Zurek mechanism) using a different process (Landau-Zener transition) containing all of the essential features of the original problem in a fully controllable manner.

III. MAPPING EVOLUTION OF QUANTUM ISING MODEL ONTO LANDAU-ZENER DYNAMICS

The physics underlying the nonequilibrium dynamics of phase transitions is a potentially vast field. It is thus of utter importance to focus on a simple yet fundamental model. The quantum Ising model is one of the prototypical many-body systems that exhibit a quantum phase transition [29]. The Hamiltonian describing a one-dimensional ferromagnetic Ising chain is defined as follows:

$$\mathcal{H}_{\text{Ising}} = -J\sum_{n=1}^{N}\left(gS_n^x + S_n^zS_{n+1}^z\right), \tag{1}$$

where S_n^x and S_n^z are the spin operators at site n and g is the applied magnetic field, N is total number of the site considered, and we assume the periodic boundary conditions $\vec{S}_{N+1} = \vec{S}_1$. There is a quantum phase transition that occurs at the critical point $g = 1$, between a paramagnetic state when applied fields dominate and a ferromagnetic state when interactions dominate. It is better to give the measure of the distance from the critical point as $\lambda = g - 1$. When the system approaches through the critical point at a finite rate $1/\tau_Q$ in the presence of a time-dependent field, the density of kinks after quenching is estimated by Kibble-Zurek theory to be [30,31]

$$\rho_{\text{KZ}} = \frac{1}{2\pi}\sqrt{\frac{\hbar}{2J\tau_Q}}. \tag{2}$$

The time evolution of the Ising model can be mapped onto a series of Landau-Zener transitions of different quasiparticle modes. We define a Jordan-Wigner transformation $S_n^x = 1 - 2C_n^+C_n$, $S_n^z = -(C_n + C_n^+)\Pi_{m<n}(1 - 2C_m^+C_m)$, where C_n^+, C_n are fermionic creation and annihilation operators, respectively, at site n. Then, using the Fourier transform $C_n = e^{-i\pi/4}\sum_k C_k e^{ikna}/\sqrt{N}$, the quantum Ising model can be decomposed into a Landau-Zener Hamiltonian for each mode with momentum k:

$$\mathcal{H}_{\text{Ising}} = \frac{1}{2}\sum_{k>0}\Psi_k^+\mathcal{H}_k\Psi_k, \quad \mathcal{H}_k = \begin{pmatrix}\epsilon_k & \Delta_k\\ \Delta_k & -\epsilon_k\end{pmatrix}, \tag{3}$$

where $\Psi_k \equiv (C_k^+, C_{-k})$, $\epsilon_k = 4J[g - \cos(ka)]$, $\Delta_k = 4J\sin(ka)$, and a is the lattice spacing of the chain.

After a Bogoliubov transformation $C_k = \alpha_k\chi_k + \beta_{-k}^*\chi_{-k}^+$, the equations of motion satisfy the standard Landau-Zener form [31]:

$$i\hbar\frac{d}{dt}\begin{pmatrix}\beta_k\\ \alpha_k\end{pmatrix} = \frac{1}{2}\begin{pmatrix}vt & 1\\ 1 & -vt\end{pmatrix}\begin{pmatrix}\beta_k\\ \alpha_k\end{pmatrix}. \tag{4}$$

It becomes increasingly apparent that the dynamical equation of the system can be mapped onto a series of Landau-Zener transitions with the velocity $v = 1/4J\tau_Q\sin^2(ka)$.

When g is ramped down to the critical point, the system is excited and the density of defects is the sum of the excitation probability $P_{\text{LZ}}(k)$ of quasiparticles with different momenta [31]:

$$\rho_{\text{KZ}} = \frac{1}{2\pi}\int_{-\pi}^{\pi}P_{\text{LZ}}(k)d(ka), \tag{5}$$

where $P_{\text{LZ}}(k)$ is the solution of the Landau-Zener problem in Eq. (4).

To be more specific, Eqs. (4) and (5) theoretically demonstrate that such quenching process in the quantum Ising model could be obtained by simulating the Landau-Zener probability $P_{\text{LZ}}(k)$ with different velocities, v, and thus the momenta, k.

IV. QUANTUM SIMULATION USING AN ELECTRON CHARGE QUBIT

The parameters of a quantum simulator system must be well controlled. In our simulation, we use an electron charge qubit trapped in a double quantum dot. Our wafer was grown by molecular-beam epitaxy, and a thin layer of electrons,

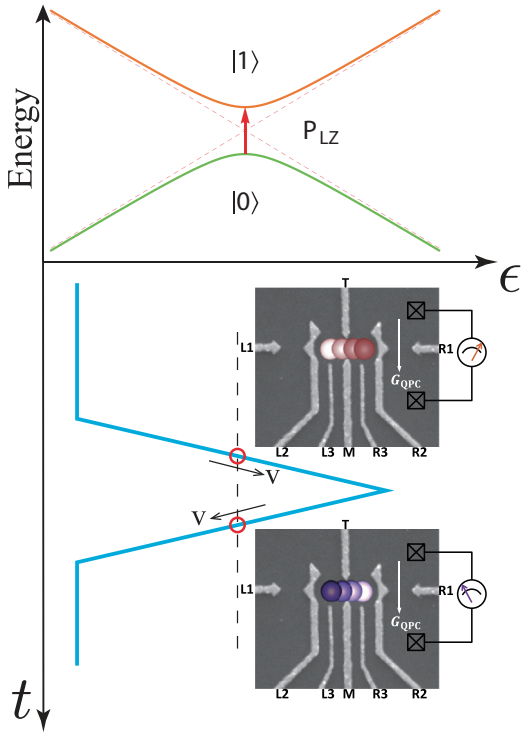

FIG. 2. (Color online) Experimental scheme used to realize the Landau-Zener transition of electron charge qubit in a double quantum dot. Left: the driving pulse control the system undergoing double-passage Landau-Zener transition process with a designed velocity. Right: scanning electron micrograph of the double quantum dot device and the quantum point contact charge sensor. The color plot of the electron represents the occupation states during the pulse sweeping.

which is referred to two-dimensional electron gas, could be formed at the interface between the AlGaAs layer and GaAs layer. Using standard Hall resistance data and Shubnikov–de Haas oscillations in the longitudinal resistance, the density and mobility of the two-dimensional electron gas were determined to be 3.2×10^{11} cm^{-2} and 1.5×10^{5} cm^2/V s, respectively. Figure 2 shows a top-down scanning electron micrograph of one of our processed double quantum dot devices. The Ti-Au electrodes were fabricated on the top surface of the wafer. The $L2$, $L3$, $R2$, $R3$, M, and T gates were used to confine the electrons in the double quantum dot, and the M and T gates could also adjust the tunnel coupling between the two dots. The left and right quantum point contacts, which were used as nearby charge detectors, were formed by the $L1$ and $L2$, $R1$ and $R2$ gates, respectively.

The quantum bit Hamiltonian in the basis of $|L\rangle$ and $|R\rangle$ consists of two terms [32,33]:

$$\mathcal{H}_{\text{qubit}} = \frac{1}{2}\begin{pmatrix} \epsilon & \Delta \\ \Delta & -\epsilon \end{pmatrix}. \tag{6}$$

The diagonal term ϵ denotes the energy-level difference of the states $|L\rangle$ and $R\rangle$, and the off-diagonal term Δ represents the interaction between the two states, depending on the tunnel coupling of the two dots. Here, we denote the electrons in the left and right dots as the states $|L\rangle$ and $|R\rangle$, respectively. The charge occupation probabilities in the double quantum dot states ($|L\rangle$ or $|R\rangle$) were measured via standard charge detection techniques [32]. Due to the strong capacitive coupling between the double quantum dot and nearby detector, the changes in the conductance G_{QPC} through the quantum point contact were sensitive to the changes in the double quantum dot charge states. We used the right quantum point contact as the sensor. In practice, we would usually repeat the procedure outlined above approximately 10^7 times to enhance the signal sensitivity. All measurements were performed in an Oxford Triton dilution refrigerator with a base temperature of 30 mK.

Our scheme for probing the Landau-Zener transition of the quantum simulator for different momenta k is illustrated in Fig. 2. An Agilent 81134A pulse generator was used to apply a controlled electric pulse with a defined amplitude and time width onto the $L3$ gate of the double quantum dot. First, we initialize the qubit to the ground state $|0\rangle$ at a negative detuning. Next, we drive the qubit in a superposition state of $|0\rangle$ and $|1\rangle$ via a linearly increasing pulse with velocity v through the anticrossing region. In the simulation, Eq. (6) is reduced to the same Landau-Zener problem indicated by Eq. (4) because the diagonal term can be tuned with a time-dependent electric field:

$$\mathcal{H}_{\text{LZ}} = \frac{1}{2}\begin{pmatrix} \epsilon_0 + vt & \Delta \\ \Delta & -(\epsilon_0 + vt) \end{pmatrix}. \tag{7}$$

Continuously adjusting the amplitude of the applied electrical pulse while keeping its time width fixed allows for the rate v to be swept over a wide range, ensuring that the Landau-Zener transition probability P_{LZ} can be investigated for different values of momentum k. Finally, we apply a linearly decreasing pulse to make the qubit pass the anticrossing point twice. This double-passage process will cause the final state of the qubit to be a combination of the nonadiabatic level transition P_{LZ} (proportional to the sweeping velocity) and accumulated phase ϕ during the adiabatic evolution (determined by the path drawn by the driving pulse from the initial detuning) [25]: $P_{|1\rangle} = 2P_{\text{LZ}}(1 - P_{\text{LZ}})(1 + \cos\phi)$ (see Appendixes for the discussion of decoherence effects and simulation fidelity estimation). The probability of finding the qubit in the excited state $|1\rangle$ is measured at far detuning where the basis is $|L\rangle$ using a nearby quantum point contact charge sensor.

Figure 3 shows the recorded charge state occupation $P_{|L\rangle}$ as a function of both the energy-level detuning ϵ_0 and the sweeping rate v. For our experiments, the tunnel coupling Δ is adjusted to 5 μeV. Oscillations known collectively as Landau-Zener-Stükelberg interference [25,27] indicate that P_{LZ} for different momentum k can be determined by monitoring information about $P_{|L\rangle}$.

In Fig. 4(a), we plot the measured $P_{\text{LZ}}(k)$ as a function of momentum k over the range $0 < ka < \pi$. In the experiment, we set the velocity v to a value corresponding to a simulated quench time of $J\tau_Q = 1$ μeV/ns. The data for different momenta can be used to obtain the defect density ρ_{KZ} based on Eq. (5), where the modes with small momenta contribute the most. The simulation discussed above can be performed for various quench times. Figure 4(b) shows the simulated ρ_{KZ} as a function of quench time, τ_Q. The experimental data are in reasonable agreement with the results of the Kibble-Zurek theory prediction Eq. (2), which are shown as a solid line. The kink density created by quenching the quantum Ising system

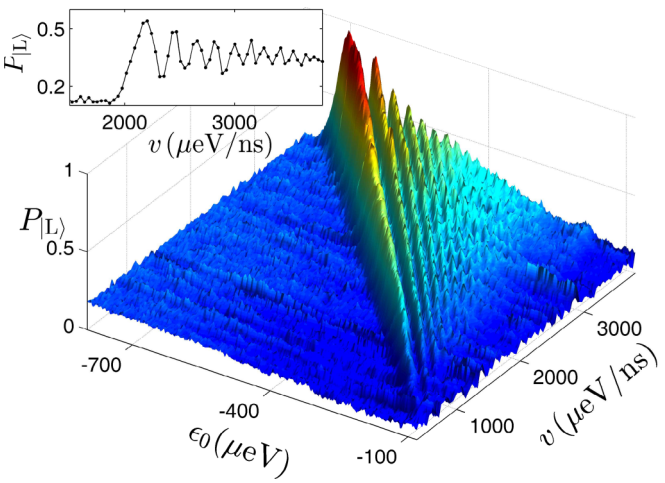

FIG. 3. (Color online) Simulation of the quenched quantum Ising model with tunable Landau-Zener dynamics. The occupation of the qubit in the excited state $|1\rangle$ (detected at far detuning where the basis is $|L\rangle$) as a function of the energy position ϵ_0 and the sweeping rate v, revealing a double-passage Landau-Zener transition process. The inset shows a line cut in Fig. 3 at a fixed $\epsilon_0 = -400$ μeV. In the experiment, applying Landau-Zener dynamics for varying sweep rates v allowed for the simulation of the dynamics of the quenched quantum Ising model for each quasiparticle mode with momentum k.

scales as $\tau_Q^{-1/2}$, precisely the same universal exponent expected by the Kibble-Zurek mechanism [30].

The quantum simulation scheme provides a useful platform with which to study not only the well-known features of the Kibble-Zurek mechanism, but also as yet unknown physics. Evolution in the mapped Landau-Zener equation (4) starts from $t_i = -\infty$ and stops at $t_f = 2J\tau_Q \sin(2ka)$. When the quench is slow (large τ_Q), the corresponding final time t_f can be safely extended to $+\infty$ implying the solution of Eq. (4) equivalent to the complete Landau-Zener transition probability $P_{\mathrm{LZ}}(k) \approx \exp(-\pi/2\hbar v)$ [31]. This usually leads to the power law $\tau_Q^{-1/2}$ of the topological excitations as Kibble-Zurek theory predicted, while for a fast quench situation (small τ_Q), the Landau-Zener process is incomplete or terminates at finite

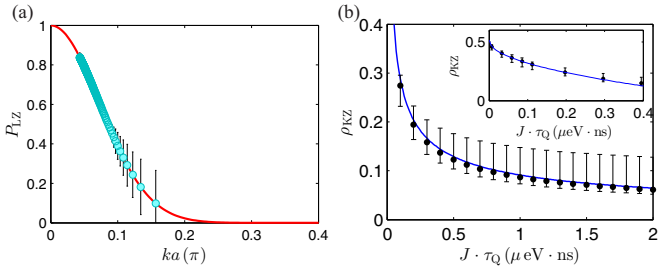

FIG. 4. (Color online) Quantum simulation of the Kibble-Zurek-like behavior of defect density as a function of quench time. (a) A typical simulation of Landau-Zener probability, P_{LZ}, for different momentum, k, extracted from Fig. 3. The solid line is a numerical fit. (b) The simulated density of defects ρ_{KZ} as a function of quench time, τ_Q. The curve represents the Kibble-Zurek theoretical prediction based on Eq. (2). The inset shows the simulation results for very fast quench regime.

ending time t_f. The simulation results for fast quench rate are displayed in the inset of Fig. 4(b), where we find a new regime characterized by a different behavior as $1/2[1 - (J\tau_Q/\hbar)^{1/2}]$. We remark that for a quenched Lipkin-Meshjov-Glich model, there is also a scaling $\tau_Q^{-3/2}$ crossover to a steeper power law τ_Q^{-2} as explained by incomplete Landau-Zener transitions [34].

V. CONCLUSION

In summary, we implemented a proof-of-principle quantum simulation to explore various properties of Ising model for a range of quench time using a designed Landau-Zener simulator. Our experiment serves as a first step toward more complex quantum simulations. It is expected that, in the near future, research will move toward the quantum simulation of dynamics that are difficult to observe in real systems (see the Appendixes for quantum simualtion of correlation functions of quantum Ising model), such as nonlinear quenching [35], or to address a broad range of quantum phase transitions that occur in more complex condensed-matter systems, for example, the XY, Kitaev, or Creutz model [36,37]. Our scheme does not use a sequence of quantum gates as in a digital quantum simulation [12–15], and the desired outcome does not appear to be affected drastically by decoherence; thus scaling to a large number of quantum dot qubits might be simpler.

ACKNOWLEDGMENTS

We would like to thank Dr. Dziarmaga for helpful discussions. This work was supported by the National Fundamental Research Program (Grant No. 2011CBA00206) and National Natural Science Foundation (Grant No. 11274294).

APPENDIX A: QUANTUM SIMULATION OF ENTROPY, CORRELATIONS, AND MAGNETIZATION

Here we demonstrate a series of quantum simulation examples for quenched quantum Ising model, notably the quantities such as entropy, magnetization, and correlation functions. These are the basic building blocks from which one can construct other physical quantities. Our strategy for the study is as follows.

First, in our simulation, the implemented algorithm establishes a mapping of a quantum Ising model onto a Landau-Zener type equation of Bogoliubov excitations with velocity $v = 1/4J\tau_Q \sin^2(ka)$, i.e., Eq. (4) in the main text. In fact, the associated density matrix contains all of the information,

$$\rho_{\mathrm{LZ}}(k) = \begin{pmatrix} |\beta_k|^2 & \beta_k\alpha_k^* \\ \alpha_k\beta_k^* & |\alpha_k|^2 \end{pmatrix}, \tag{A1}$$

in which the elements of the density matrix are constructed by the solution of the Landau-Zener equation. Therefore, the density matrix $\rho_{\mathrm{LZ}}(k)$ can be directly obtained from the Landau-Zener transition probability and phase by measuring Landau-Zener-Stükelberg interference pattern of the qubit for different velocities v. The raw experimental results are shown in Figs. 3 and 4(a) in the main text.

Secondly, the quenching dynamics of the spin model can be viewed as a superposition of different configurations. In other words, the final state for the block of N-spin quantum Ising

chain is described by a density matrix of the product form

$$\rho_{\text{Ising}} = \otimes\rho_{\text{LZ}}(k) = \begin{pmatrix} A & B^{+} \\ B & 1-A \end{pmatrix}. \tag{A2}$$

Here A and B are N-dimensional matrices, and their elements are defined as quadratic correlators of the fermionic creation and annihilation operators C_n^{+}, C_n at site n: $A_{m,n} \equiv \langle C_m C_n^{+}\rangle = \frac{1}{2\pi}\int_{-\pi}^{\pi} |\beta_k|^2 \exp[ika(m-n)]d(ka)$ and $B_{m,n} \equiv \langle C_m C_n\rangle = \frac{1}{2\pi i}\int_{-\pi}^{\pi} \beta_k\alpha_k^{*} \exp[ika(m-n)]d(ka)$. By measuring the set of Landau-Zener processes for a range of simulated momentums k, the full state density matrix ρ_{Ising} can be reconstructed from the signal of the probe qubit.

With complete knowledge of the density matrix ρ_{Ising}, we can determine all of the macroscopic observables. For example, an expression for the entropy follows as $S = -\text{Tr}\rho_{\text{Ising}}\log_2\rho_{\text{Ising}}$, which can be used as a tool to probe quantum phase transitions in many-body systems. Apart from the entropy, correlation functions after a quench are of fundamental interest because they provide a direct manifestation of the universal properties of a phase transition. In this study, we are particularly interested in investigating the transverse magnetization for slow quench:

$$M = \langle S_n^{x}\rangle = \langle 1 - 2C_n^{+}C_n\rangle \approx \frac{1}{\pi}\int_{-\pi}^{\pi} P_{\text{LZ}}(k)d(ka). \tag{A3}$$

Thus the magnetization can be simulated for a range of the probed quench time τ_Q. It is clear that the magnetization decays to zero when the quench time is varied to a large value, a characteristic of the ferromagnetic ground state after a quench.

To summarize, we employed a designed Landau-Zener processor using semiconductor qubits to explore various quantities of Ising system for a range of quench time. We would like to emphasize that in order to detect experimentally the density of excitations generated by passing through a critical point in a realistic system, it is a challenge that one should distinguish between situations where such excitations are long-lived quasiparticles or decay after being created. However, these quantities are generally directly accessible experimentally in our quantum simulations presented here.

APPENDIX B: DECOHERENCE EFFECT AND FIDELITY ESTIMATION

The simulator dynamics in the main text can be seen as a sequence of Landau-Zener transition and adiabatic evolution. In the so-called adiabatic-impulse model [25], Landau-Zener transition at anticrossings is treated as P_{LZ} and the dynamics phase ϕ is determined by the path drawn by the system in energy-level space. Putting things together, we can calculate the excitation probability after the driving pulse starting from the ground state, as given by

$$P_{|1\rangle} = 2P_{\text{LZ}}(1 - P_{\text{LZ}})(1 + \cos\phi). \tag{B1}$$

This probability oscillates known collectively as Landau-Zener-Stükelberg interference [25,27]. The dynamics discussed above is a unitary and coherent process. However, in any experimental implementation the undesired and unavoidable coupling to external degrees of freedom leads to decoherence and thus it affects the observed simulator behavior. To model the experimental results in Fig. 3, we include the decoherence time T_2 and fit the oscillations to a phenomenological damped cosine form [32].

The dissipative dynamics of the simulator is also numerically obtained by solving the time-dependent master equations of the density matrix as follows:

$$\frac{d\rho}{dt} = -\frac{i}{\hbar}[\rho, H] + L, \tag{B2}$$

in which H is the Hamiltonian introduced in Eq. (6) in the main text. The standard Lindblad form L describes the incoherent process proportional to the relaxation and dephasing time [38,39]. The calculated solutions are in reasonable agreement with the experimental results (Fig. 3 in the main text).

Furthermore, we can estimate the simulation fidelity of each pulse induced simulator dynamics [40]. The fidelity is defined as $F = \text{Tr}[\sqrt{\rho_i}\rho_r\sqrt{\rho_i}]$, in which ρ_i is the density matrix of the desired ideal state and ρ_r is that of the real final state [40–43]. During the simulation, the interactions of the simulator with its environment lead to a loss of fidelity. Thus the fidelity depends on the specific properties of the working parameters. For the sake of simplicity let us consider an example: a simulation experiment for the designed velocity $v = 2400\ \mu\text{eV/ns}$, initial detuning $\epsilon_0 = -400\ \mu\text{eV}$, and decoherence time $T_2 = 1$ ns. From a comparison of the ideal predicted signal and the measured signal after a simulation, we can estimate a fidelity of 83% in the present work. In addition, using more advanced optimization methods to extend the decoherence time, the fidelity higher than 95% can be expected.

[1] T. W. B. Kibble, J. Phys. A **9**, 1387 (1976).
[2] W. H. Zurek, Nature (London) **317**, 505 (1985).
[3] P. C. Hendry *et al.*, Nature (London) **368**, 315 (1994).
[4] C. Bauerle *et al.*, Nature (London) **382**, 332 (1996).
[5] V. M. H. Ruutu *et al.*, Nature (London) **382**, 334 (1996).
[6] L. E. Sadler *et al.*, Nature (London) **443**, 312 (2006).
[7] R. Yusupov *et al.*, Nat. Phys. **6**, 681 (2010).
[8] K. Pyka *et al.*, arXiv:1211.7005.
[9] S. Ulm *et al.*, arXiv:1302.5343.
[10] S. Trotzky *et al.*, Nat. Phys. **8**, 325 (2012).
[11] A. Polkovnikov *et al.*, Rev. Mod. Phys. **83**, 863 (2011).
[12] I. Buluta and F. Nori, Science **326**, 108 (2009).
[13] I. Bloch, J. Dalibard, and S. Nascimbene, Nat. Phys. **8**, 267 (2012).
[14] R. Blatt and C. F. Roos, Nat. Phys. **8**, 277 (2012).
[15] A. Aspuru-Guzik and P. Walther, Nat. Phys. **8**, 285 (2012).
[16] J. Dziarmaga, Adv. Phys. **59**, 1063 (2010).
[17] A. A. Houck, H. E. Tureci, and J. Koch, Nat. Phys. **8**, 292 (2012).
[18] J. Sabbatini, W. H. Zurek, and M. J. Davis, Phys. Rev. Lett. **107**, 230402 (2011).

[19] A. J. Daley, H. Pichler, J. Schachenmayer, and P. Zoller, Phys. Rev. Lett. **109**, 020505 (2012).
[20] O. Viehmann, J. von Delft, and F. Marquardt, Phys. Rev. Lett. **110**, 030601 (2013).
[21] B. Damski, Phys. Rev. Lett. **95**, 035701 (2005).
[22] B. Damski and W. H. Zurek, Phys. Rev. A **73**, 063405 (2006).
[23] L. D. Landau and E. M. Lifshitz, *Quantum Mechanics* (Pergamon, London, 1958).
[24] C. Zener, Proc. R. Soc. A **137**, 696 (1932).
[25] S. N. Shevchenko, S. Ashhab, and F. Nori, Phys. Rep. **492**, 1 (2010).
[26] W. D. Oliver *et al*., Science **310**, 1653 (2005).
[27] J. R. Petta, H. Lu, and A. C. Gossard, Science **327**, 669 (2010).
[28] G. Cao *et al*., Nat. Commun. **4**, 1401 (2013).
[29] S. Sachdev, *Quantum Phase Transitions* (Cambridge University Press, Cambridge, UK, 2001).
[30] W. H. Zurek, U. Dorner, and P. Zoller, Phys. Rev. Lett. **95**, 105701 (2005).
[31] J. Dziarmaga, Phys. Rev. Lett. **95**, 245701 (2005).
[32] K. D. Petersson, J. R. Petta, H. Lu, and A. C. Gossard, Phys. Rev. Lett. **105**, 246804 (2010).
[33] T. Hayashi, T. Fujisawa, H. D. Cheong, Y. H. Jeong, and Y. Hirayama, Phys. Rev. Lett. **91**, 226804 (2003).
[34] T. Caneva, R. Fazio, and G. E. Santoro, Phys. Rev. B **78**, 104426 (2008).
[35] D. Sen, K. Sengupta, and S. Mondal, Phys. Rev. Lett. **101**, 016806 (2008).
[36] K. Sengupta, D. Sen, and S. Mondal, Phys. Rev. Lett. **100**, 077204 (2008).
[37] A. Bermudez, D. Patane, L. Amico, and M. A. Martin-Delgado, Phys. Rev. Lett. **102**, 135702 (2009).
[38] M. A. Nielsen and I. L. Chuang, *Quantum Computation and Quantum Information* (Cambridge University Press, Cambridge, UK, 2000).
[39] D. Press *et al*., Nature (London) **456**, 218 (2008).
[40] P. Hauke *et al*., Rep. Prog. Phys. **75**, 082401 (2012).
[41] P. Rabl *et al*., Nat. Phys. **6**, 602 (2010).
[42] C. Piermarocchi, P. Chen, Y. S. Dale, and L. J. Sham, Phys. Rev. B **65**, 075307 (2002).
[43] S. E. Economou, L. J. Sham, Y. Wu, and D. G. Steel, Phys. Rev. B **74**, 205415 (2006).